Proceedings of ASME Turbo Expo 2011
GT2011
June 6-10, 2011, Vancouver, British Columbia, Canada

GT2011-46500

DEPENDENCY OF UNSTEADY TIME-LINEARIZED FLUTTER INVESTIGATIONS ON THE STEADY STATE FLOW FIELD

Michael Blocher
Institute of Aeroelasticity
DLR – German Aerospace Center
Bunsenstr. 10, 37073 Göttingen
Germany
Email: michael.blocher@dlr.de

Markus May
Institute of Aeroelasticity
DLR – German Aerospace Center
Bunsenstr. 10, 37073 Göttingen
Germany
Email: markus.may@dlr.de

Harald Schoenenborn
Compressor Aerodynamics/Aeroelasticity
MTU Aero Engines GmbH
Dachauer Str. 665, 80995 München
Germany
Email: harald.schoenenborn@mtu.de

ABSTRACT

The influence of the steady state flow solution on the aeroelastic stability behaviour of an annular compressor cascade shall be studied in order to determine sensitivities of the aerodynamic damping with respect to characteristic flow parameters. In this context two different flow regimes – a subsonic and a transonic case – are subject to the analysis.

The pressure distributions, steady as well as unsteady, on the blade surface of the NACA3506 profile are compared to experimental data that has been gained by the Institute of Aeroelasticity of the German Aerospace Center (DLR) during several wind tunnel tests at the annular compressor cascade facility RGP-400 of the Ecole Polytechnique Fédérale de Lausanne (EPFL). Whereas a certain robustness of the unsteady CFD results can be stated for the subsonic flow regime, the transonic regime proves to be very sensitive with respect to the steady state solution.

NOMENCLATURE

C_p	pressure coefficient
$\vec{F}_c$, $\vec{F}_v$	convective and viscous flux vector
K	generalized stiffness matrix
M	generalized mass matrix
N	number of blades, here $N = 20$
$\vec{R}$	residual vector
$\vec{S}$	source term vector
$\vec{U}$	vector of conservative variables
V	cell volume
$\vec{f}_i$	aerodynamic forces
j	imaginary unit
p	pressure
$\vec{q}_i$	individual generalized coordinates
t	time
$\vec{x}$	position of mesh points
x/c	relative chord length
Λ_{AERO}	logarithmic decrement of aerodynamic damping
Φ	phase angle with respect to blade motion
α	angular amplitude of the blade motion
ϕ	structural modal basis
σ_n	inter-blade phase angle (IBPA), $\sigma_n = \frac{2\pi n}{N}$
ω	angular frequency of vibration, $\omega = 2\pi f$

Indices and other notations

$_0$	steady state value
$_1$	average static value at inlet
$_{t_1}$	average total value at inlet
$\hat{}$	complex amplitude
^{H}	hermitian
$\Re(\,)$	real part of ( )

INTRODUCTION

Due to the reduction of computational costs time-linearized CFD codes are widely used to assess the aeroelastic stability of turbomachinery bladings in the industrial design process. One of the first implementations by HALL [1] was based on solving the linearized Euler equations to analyze the unsteady flow in turbomachinery. Further developments (e.g. HOLMES AND LORENCE [2], CLARK AND HALL [3], SBARDELLA AND IMREGUN [4] or CAMPOBASSO AND GILES [5]) extended this approach to two- and three-dimensional viscous flow regimes, by solving the linearized Navier-Stokes equations for flutter calculations.

All of these methods are based on the assumption of small time-harmonic perturbations of the flow field due to a harmonic motion of the rotor blades according to the eigenmode of interest. The respective system of linear equations is solved in the frequency domain. Often, in this context, general remarks are given saying that the amplitude or the perturbation has to be ”sufficiently” small. Of course, this limits the application domain of linear solvers when dealing with nonlinear flow physics.

However, no investigations have been performed so far with regard to the accuracy of the underlying steady-state solution. It seems evident that the steady Navier-Stokes solution for the operating point at which the linearization is performed is of major importance with regard to the corresponding unsteady results. Exactly this subject shall be addressed in the present paper by the comparison of unsteady time-linearized pressure distributions (based on different steady state solutions) with experimental results for an annular compressor cascade. The mentioned steady state solutions are generated by varying the parameters total inlet pressure, outlet pressure, angle of attack and leakage mass flow. For the transonic case, the sensitivities of the aerodynamic damping are calculated with respect to these four parameters. This shall shed light on the dependency of the time-linearized results on the underlying steady state flow solution.

THEORETICAL CONCEPTS

Aeroelastic Modeling

The governing aeroelastic equations of motion in generalized blade coordinates $\vec{q}_i$ yield

$$M\ddot{\vec{q}}_i(t)+K\vec{q}_i(t)=\phi^H \vec{f}_i(t), \tag{1}$$

where M and K are generalized mass and stiffness matrix respectively. Structural damping has already been neglected in Eqn. (1). For a detailed derivation please refer to the AGARD Manual on ”Aeroelasticity in Axial-Flow Turbomachines” [6].

It shall be mentioned that in this generalized modal form the equations of motion represent energy equations, where the generalized aerodynamic forces (GAF) on the right-hand side express the work done by the motion induced unsteady aerodynamic loads in the displacements of the individual mode shapes $\vec{\phi}_i^{(r)}$ for $r=1,2,...,R$.

The vector of unsteady aerodynamic forces acting on the i-th blade depends on its own blade motion as well as on its neighbours'. The time history of these movements is taken into account by the inter-blade phase angle (IBPA)

$$\sigma_n=\frac{2\pi n}{N} \quad \text{with} \quad n=0,1,\ldots,N-1. \tag{2}$$

This fundamental concept formulated by LANE [7] describes a traveling wave in which all N blades are oscillating harmonically with a certain (constant) phase shift of σ_n, whereas mode shape and vibration frequency are identical.

Time-Linearization

The TRACE code – developed at the DLR Institute of Propulsion Technology for internal flows, especially in turbomachinery – has been applied to perform the steady Reynolds-averaged Navier-Stokes (RANS) computations in this article.

The general system of conservation laws yields

$$\frac{\partial\vec{U}}{\partial t}+\frac{\partial\vec{F}_i(\vec{U})}{\partial x_i}+\vec{S}(\vec{U})=\vec{0}, \tag{3}$$

where $\vec{U}$ denotes the state vector of conservative variables, $\vec{F}(\vec{U})=\vec{F}_c(\vec{U})-\vec{F}_v(\vec{U})$ and $\vec{S}(\vec{U})$ the fluxes and source terms, respectively. To address aeroelastic problems with a moving mesh Eqn. (3) has to be rewritten in Arbitrary Lagrangian Eulerian (ALE) formulation before the spatial discretization in finite volumes is carried out:

$$\frac{\partial(V\vec{U})}{\partial t}+V\vec{R}(\vec{U},\vec{x},\dot{\vec{x}})=\vec{0}, \tag{4}$$

where V shall indicate the cell volume that varies in time. The residual $\vec{R}$ depends on the flow variables $\vec{U}$ as well as on the grid coordinates $\vec{x}$ and velocities $\dot{\vec{x}}$ in order to account for the additional fluxes due to mesh deformation.

At the DLR Institute of Aeroelasticity, first time-linearized solvers have been developed by HAGENAH [8] and PETRIE-REPAR [9]. This finally led to an integration in the environment of the TRACE code (KERSKEN ET AL. [10]).

Based on the assumption of small harmonic perturbations, the coordinates of the grid vertices $\vec{x}$ as well as the flow solution can be decomposed in a steady part (time-independent) and a time-dependent harmonic perturbation:

$$\vec{x}(t)=\vec{x}_0+\Re\left(\hat{\vec{x}}(\vec{x}_0)e^{j\omega_0 t}\right) \tag{5}$$

$$\vec{U}(\vec{x}_0,t)=\vec{U}_0(\vec{x}_0)+\Re\left(\hat{\vec{U}}(\vec{x}_0)e^{j\omega_0 t}\right) \tag{6}$$

where ω_0 is again the angular frequency of the considered mode.

Taking into account a linearized approximation of the nonlinear residual and introducing Eqn. (6) in Eqn. (4) finally results in the following system of linear equations:

$$\left(j\omega_0 + \frac{\partial \vec{R}}{\partial \vec{U}}\right)\hat{\vec{U}} = -\left(\frac{\partial \vec{R}}{\partial \vec{x}}\hat{\vec{x}} + \frac{\partial \vec{R}}{\partial \dot{\vec{x}}} j\omega_0 \hat{\vec{x}} + j\omega_0 \frac{\hat{V}}{V_0}\vec{U}_0\right). \quad (7)$$

It shall be mentioned that the turbulence model has not been linearized; the constant eddy viscosity assumption was used instead, which might not be suitable for complex flow conditions with separation.

The difference between this approach and the time-linearized Euler Lin3D method developed by KAHL [11] is the neglect of viscous flow contributions $\frac{\partial \vec{F}_v}{\partial \vec{U}}$ in the implementation of the term $\frac{\partial \vec{R}}{\partial \vec{U}}$ on the one hand and the interpolation of the steady flow solution on a coarser Euler mesh on the other hand. Nevertheless, the application of a linearized Euler method on a steady Navier-Stokes solution is justified by the assumption that the perturbations detected by a time-linearized Euler solver propagate on the characteristics of the steady Navier-Stokes flow field.

EXPERIMENTAL SETUP

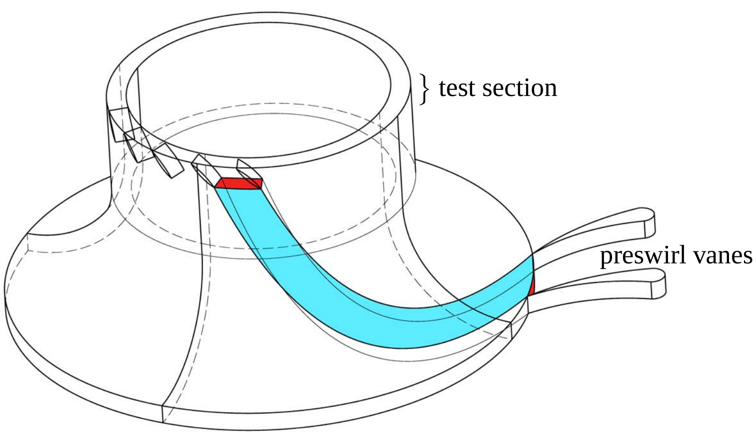

FIGURE 1. SCHEMATIC OF THE AIR FLOW IN THE ANNULAR CASCADE AT THE EPFL

Submitting a rotating system to wind tunnel tests is extremely complex regarding drive system (without flow obstruction) and data extraction (high data rate for unsteady experiments). Therefore, the annular cascade RGP-400 of the "Laboratoire de Thermique appliquée et de Turbomachines" (LTT) at the "Ecole Polytechnique Fédérale de Lausanne" (EPFL) [12] uses an inverse approach. In this kind of wind tunnel, the rotor is static and the air flow is rotated by means of inlet guide vanes (Fig. 1). The data can then be extracted via the center of the cascade.

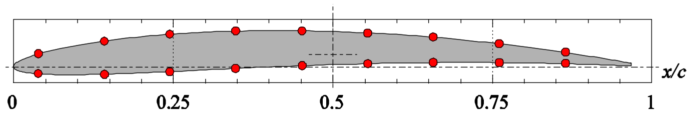

FIGURE 2. SCHEMATIC OF THE STEADY STATE PRESSURE TAPS ON THE BLADE SURFACE

During the experiments carried out by the DLR Institute of Aeroelasticity, the steady state conditions were measured with pressure taps. Those were distributed on blade cross sections at 20%, 50% and 80% channel height on six of the 20 blades with NACA3506 profiles of the compressor cascade (Fig. 2). The inflow and outflow conditions were measured with five-hole-probes a certain distance in front of the leading edges and behind the trailing edges of the blades.

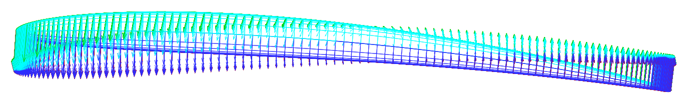

FIGURE 3. 1^{ST} ROTATIONAL EIGENMODE OF THE TEST BLADE

Then, the blades were excited to vibrations in their first rotational eigenmode (Fig. 3). The blade mounting was manufactured as to allow for this. The necessity of a blade motion resulted in gaps in the inner wall of the arrangement that connected a void (cavity) below the blade base with the flow channel.

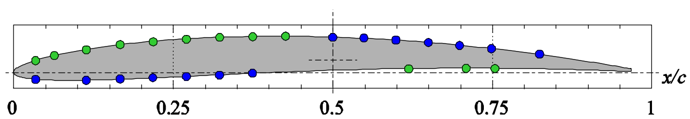

FIGURE 4. SCHEMATIC OF THE PIEZO-RESISTANT PRESSURE SENSORS ON THE BLADE SURFACE

During the unsteady experiments, data was gathered on four different blades at 50% channel height with piezo-resistant pressure sensors (Fig. 4). The results of these measurements were then combined to yield the unsteady pressure distribution around one blade. See BELZ ET AL. [13, 14] for more details.

A combination of the unsteady pressure values obtained from these forced motion experiments with the blade motion resulted in a pressure distribution in amplitude and phase angle. The calculation of the aerodynamic work on the blade due to these unsteady pressure distributions indicates if the blade is excited or damped.

NUMERICAL INVESTIGATION

The DLR in-house code TRACE [15] was used to establish a steady state flow simulation of a subsonic (Ma = 0.74) and a transonic (Ma = 0.85) flow case investigated during the experiments. Therefore, the current work forms an extension to the work done by KEMME [16]. In KEMME'S work, just the main flow region was modeled. Since then, computing power and modeling capabilities have developed, therefore it was possible to model the complete cavity below the blade arrangement for this simulation (Fig. 5). Apart from that, the linear module within TRACE has been used to perform the flutter computations. Previous results presented by KEMME applied a conventional nonlinear approach and referred to a different measurement campaign.

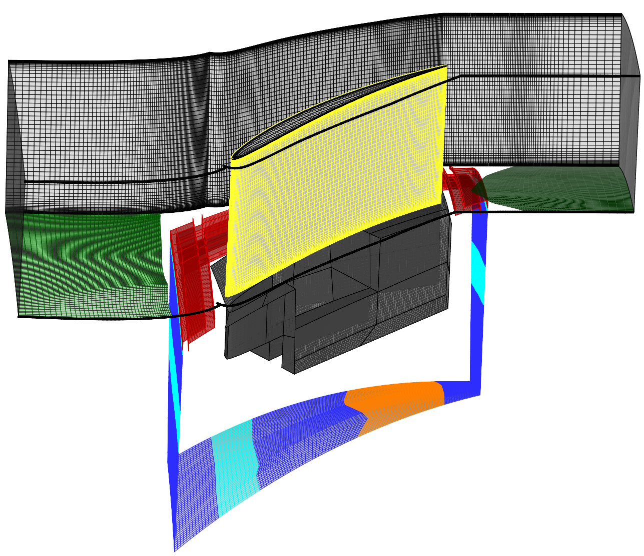

FIGURE 5. VISUALIZATION OF THE SIMULATED FLOW DOMAIN (SINGLE PASSAGE)

The used computational grid was block structured and cell centered and consisted of 2 449 844 nodes (1 633 152 nodes for the main flow path, 608 196 for the gaps between main flow path and cavity (highlighted red in Fig. 5) and 208 496 for the main cavity). The dimensionless wall distance y^+ was around 3 on the blade surface and wall functions were applied. The high number of cells used to discretize the flow domain was necessary to guarantee a mesh independent solution, especially with respect to previous investigations on the resolution of unsteady shock motion.

To reproduce the results of the steady state experiments as correctly as possible, four parameters were varied. On the basis of the steady state solution that had the best agreement with the experiment (CASE1 in Fig. 6 & 19), unsteady time-linearized simulations were performed with the linear Navier-Stokes module of TRACE and the linear Euler code Lin3D from MTU Aero Engines, Munich. To investigate the sensitivity of the linearized unsteady solution for variations of the steady state solution, two extra cases with different steady state solutions were simulated (CASE2 & CASE3). In the graphs, the abbreviation PS denotes the pressure side, SS the suction side, EPFL denotes the experimental pressure values and TRACE the steady simulation results generated by nonlinear TRACE. 20%, 50% and 80% denote the relative channel height at which the pressure on the blade surface was extracted.

The boundary conditions used were:

- Periodic boundary conditons at the sides of the single blade passage for main flow path, gaps and cavity for the steady state simulations. For the time-linearized simulations, a phase lag according to IBPA was applied.
- Viscous wall modeling (Stokes) with wall functions was applied on all walls (also in the cavity).
- At the outlet, an average static pressure was imposed (non-reflecting).
- At the inlet, a radial distribution of total pressure, total temperature, angle of attack, turbulence intensity and turbulent length scale was imposed (non-reflecting).
- Since the cells at the gap-main flow region interface do not match, zonal interface conditions were applied.

Subsonic Case (Ma = 0.74)

Four parameters not explicitly known from the experiments with a large influence on the steady state solution were identified:

- A leak mass flow in the cavity with unknown magnitude was discovered by KAHL AND HENNINGS [17]. To determine its magnitude, a leak mass flow was introduced in the simulation and its magnitude varied. To model this leak flow, a predefined flow vector is imposed on the leak surface. The magnitude of the overall leak flow is specified (between 0% - 0.4% of overall mass flow). In Fig. 5, the leak region is highligthed orange. Experiments were made concerning the position of the leak region (light blue in Fig. 5), but no effect on the steady state solution in the main flow region was determined.
- Also, the accuracy of the inflow angle determined with the miniature five hole probes was doubtful (angle accuracy of the probes, determination of the flow angle via trigonomet-

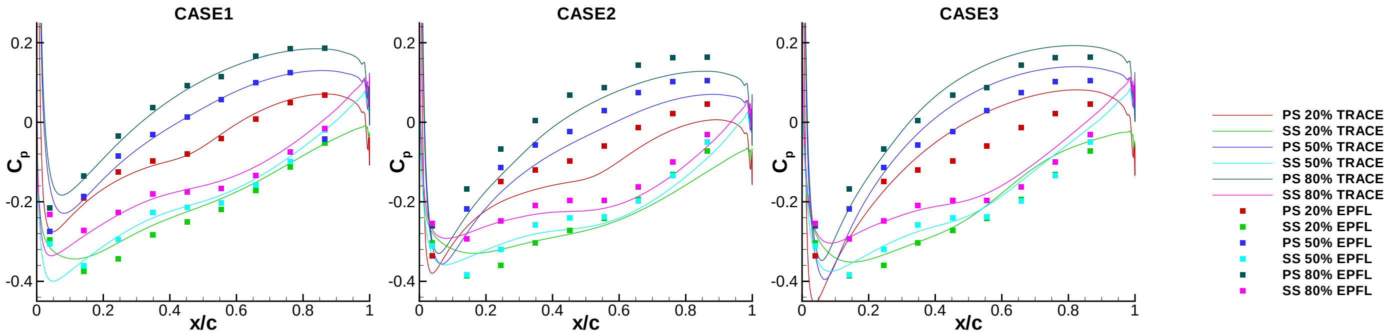

FIGURE 6. BEST CASE (CASE1), LESS ACCURATE CASE (CASE2) AND LESS ACCURATE CASE WITHOUT CAVITY MODELING (CASE3) (SUBSONIC CASE)

ric functions). Therefore, the angle of attack was varied between $\pm 1^\circ$ in small steps for the whole slightly inhomogeneous radial inlet distribution.

- During the experiments it was only possible to measure the inlet conditions between 15% and 85% of the channel height. These were used as inflow conditions (except for the angle of attack). Therefore, no data was available for the area of the inlet between 0% - 15% and 85% - 100% of the channel height. The measured data was extrapolated to the wall with a dip in total pressure in the boundary layer. As parameter variation, the total pressure in these regions was varied by up to 6 kPa in small steps.
- Lastly, the outlet pressure measured during the experiments was not usable since it was measured too near the blade trailing edge to be applicable in CFD, since TRACE assumes circumferential homogeneity. (The static pressure rises along the flow path due to wall friction and deceleration of the flow. Therefore the averaged static pressure of the experiment cannot be used as outlet pressure for the calculation and needs to be found. The static pressure variation to the experiment was testet up to 7% change compared to the experiment.)

It was established, that modeling the cavity results in much more accurate simulation results than just modeling the main flow channel (Fig. 6 & 19). From these results, it can be concluded that cavity modeling is important for large cavities that can lead to a significant bypass flow.

Steady State Simulation. The variation of the four parameters resulted in dependencies of the steady state flow solution of the different parameters.

- Both the variation of the leak mass flow in the cavity and the variation of the total inlet pressure between 0% - 15% and 85% - 100% result in a more or less prominent dip of the pressure on the blade surface near the leading edge (Fig. 7 & 9). This can be described to the increased mass flow and the necessity for a higher acceleration around the front part of the blade (C_p for the leak mass flow variation has been calculated with the inlet values of the moderate case for all three cases to preserve the differences in pressure variation).
- The variation of the angle of attack results in a variation of the difference between the pressures on the pressure side and on the suction side of the blade (Fig. 8). A higher angle of attack results in a stronger dip of the pressure on the pressure side of the blade since the air is accelerated more on the pressure side of the blade. A lower angle of attack results in a stronger dip on the suction side of the blade because the curvature of the blade causes an increased velocity on the suction side of the blade.
- The variation of the exit static pressure is directly related to the pressure on the surface of the blade (Fig. 10). A change in static pressure at the outlet changes the velocity of the flow passing the blade. Therefore, the pressure on the blade is higher for higher outlet pressures (lower velocity, lower ratio of dynamic pressure to total pressure) and lower for lower outlet pressures (higher velocity, higher ratio of dynamic pressure to total pressure). C_p has been calculated with the inlet values of the moderate casefor all three cases to preserve the differences in pressure variation.

A combination of the variation of these four parameters resulted in a flow case that was in very good accordance with the experimental results obtained for the flow field at the EPFL (Fig. 6, CASE1 & Fig. 11). Considering the character of the flow on the blade surface (Fig. 11), the authors assumed that the constant eddy viscosity assumption holds true for the flow around the profile (no flow separation).

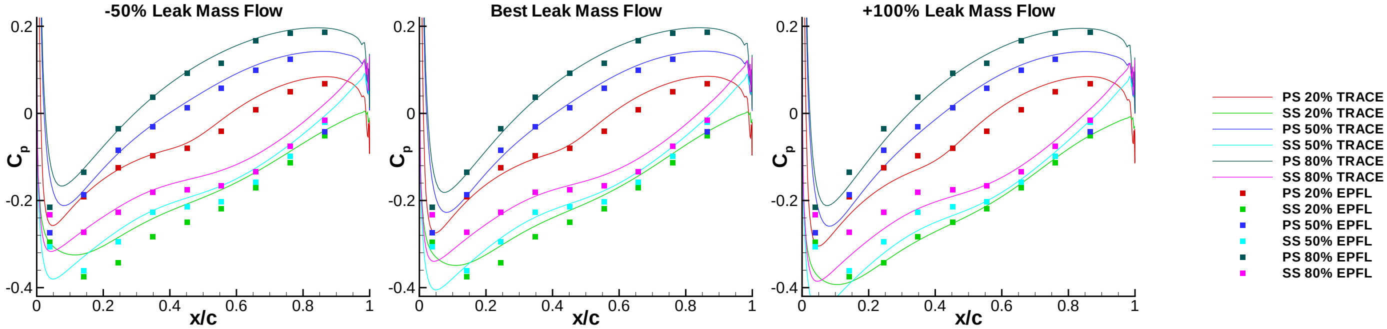

FIGURE 7. CONSEQUENCES OF A LEAK MASS FLOW VARIATION IN THE CAVITY (SUBSONIC CASE)

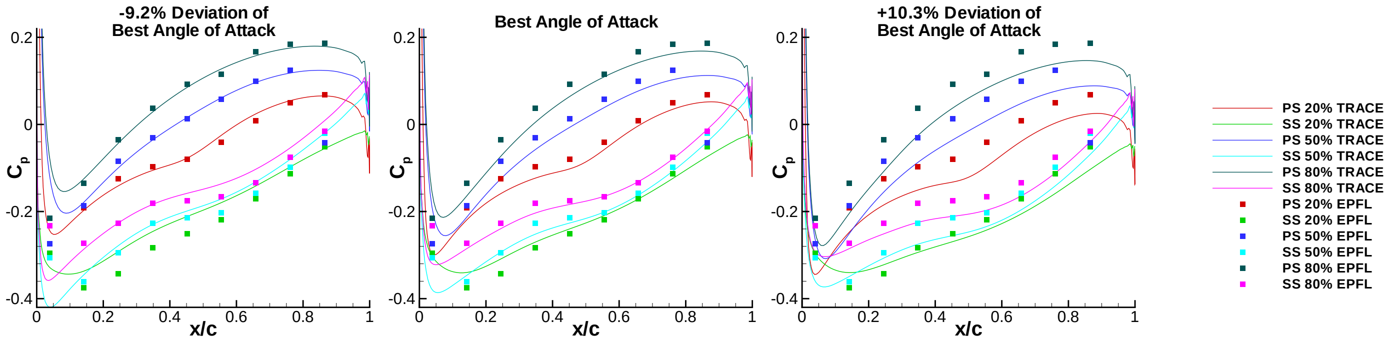

FIGURE 8. CONSEQUENCES OF AN ANGLE OF ATTACK VARIATION (SUBSONIC CASE)

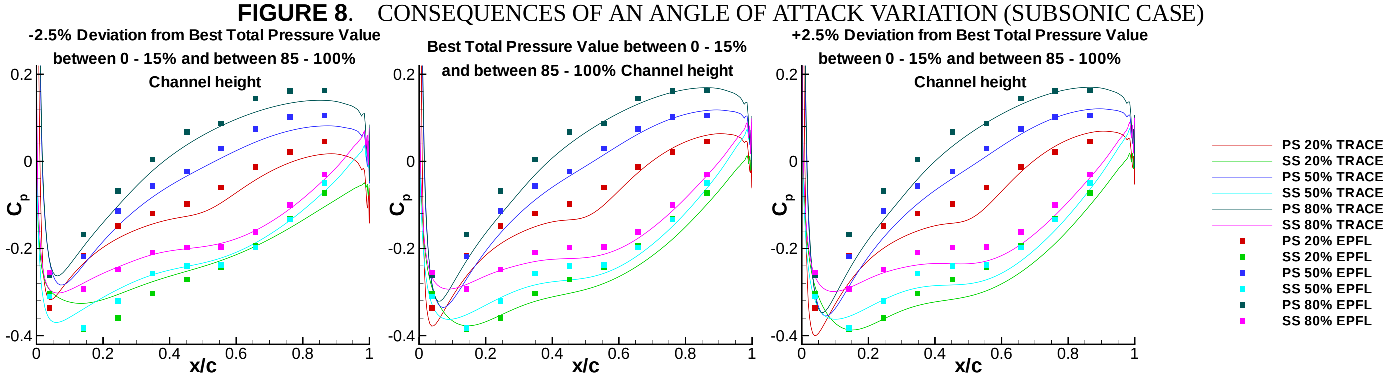

FIGURE 9. CONSEQUENCES OF A VARIATION OF THE TOTAL PRESSURE AT PARTS OF THE INLET (SUBSONIC CASE)

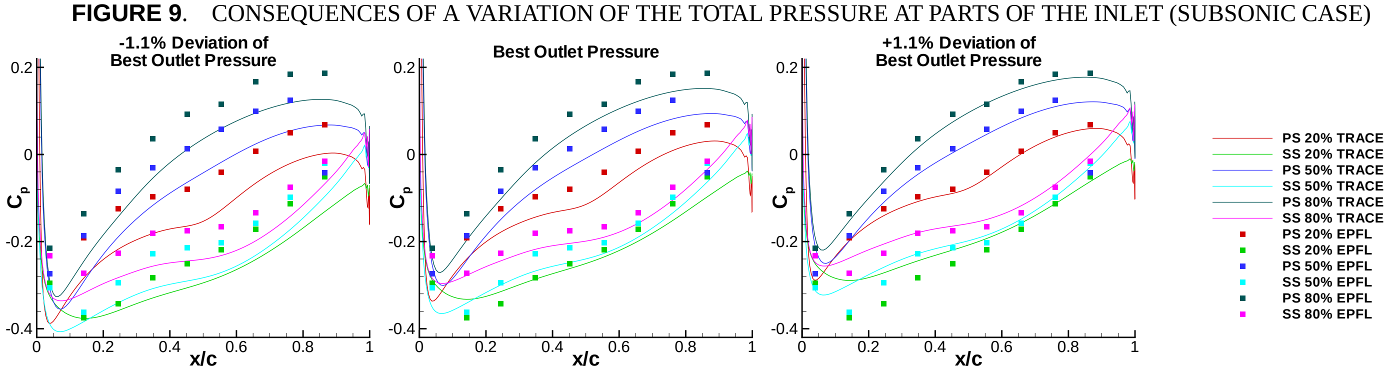

FIGURE 10. CONSEQUENCES OF AN EXIT PRESSURE VARIATION (SUBSONIC CASE)

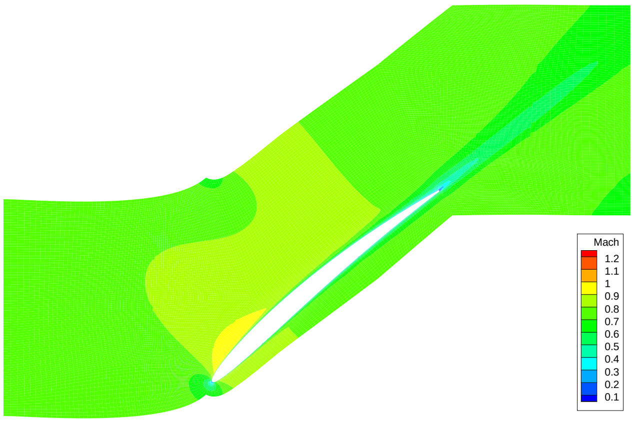

FIGURE 11. MACH NUMBER DISTRIBUTION AT 50% CHANNEL HEIGHT (SUBSONIC CASE)

Unsteady Time-Linearized Simulations. On the basis of the obtained best steady state result, a time-linearized unsteady simulation was performed with the linear module of TRACE (CASE1). For all simulations, the first eigenmode shape of the blade mounting was obtained via FEM and then mapped onto the computational grid (Fig. 3). Additionally a second time-linearized simulation was run with a steady state solution that was obtained with less accurate inlet (-1.7% deviation of total inlet pressure between 0% - 15% and between 85% - 100% channel height from CASE1 and no angle of attack variation) and outlet conditions (-2.5% deviation of static pressure value from CASE1) as well as without leak mass flow in the cavity (CASE2). The third time-linearized simulation (CASE3) was based on a steady state solution that was obtained with the same inlet and outlet conditions as CASE2 but without cavity modeling, hence a much less accurate steady state solution. At MTU in Munich, comparison calculations based on CASE1 were run with the Lin3D code. The results are shown as comparison between linearized RANS and linearized Euler codes.

Since the amplitude of the blade motion was different for experiment and simulation, the unsteady pressure coefficient was used to compare the results. It is defined as:

$$\hat{C}_p = \frac{\hat{p}}{\hat{\alpha}\,(p_{t_1} - p_1)} \tag{8}$$

The results of those three simulations for the unsteady pressure distribution at 50% channel height are presented for two IBPAs in Fig. 13 (All 20 IBPAs were simulated, but only two of them were selected for presentation.). The results of all the time-linearized simulations were analyzed for the absolute value of the unsteady pressure coefficient $\hat{C}_p$ and the phase angle between blade motion and pressure fluctuation Φ. The IBPA 180° shows a very good agreement of the time-linearized results of CASE1 with the experimental results. CASE2 is very similar to the solution of CASE1. CASE3 with the least accurate steady state solution shows already a large discrepancy to the experiment and to the other two solutions. The Lin3D solution shows that a linearized Euler approach based on an accurate RANS steady state solution is about as accurate as a time-linearized RANS approach based on a steady state solution that is a little off.

For IBPA 0°, it can be stated that even the two cases with very accurate steady state solutions are inaccurate on the pressure side of the blade regarding the phase angle between blade oscillation and pressure response. Although there is no physical explanation for the moment, the authors did not want to hold back this case that has by far the worst accordance with the experimental data. Interestingly, the omitted viscosity terms seem to overcompensate the inaccuracy of the phase angle in Lin3D where the RANS approach fails to deliver physical results.

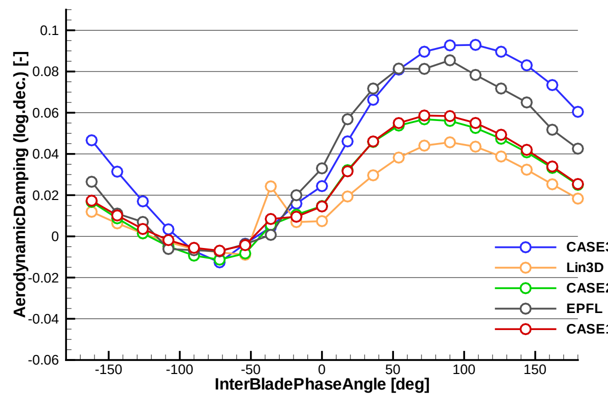

FIGURE 12. COMPARISON OF THE LOG.-DEC. OF AERODYNAMIC DAMPING OF THE FOUR TEST CASES (SUBSONIC CASE)

Via the local aerodynamic work and its integration over the blade surface, the logarithmic decrement of aerodynamic damping Λ_{AERO} can be calculated (Fig. 12). For Λ_{AERO} of the experimental case, it was assumed that the measured pressure values at 50% channel height are valid for the whole blade height and along the profile contour between two points. This is a rough assumption but leads to results that are in the same order of magnitude as the simulated values. The strong resemblance of CASE3 and the experimental damping curve is no surprise: the cross section data at 50% channel height has been considered representative for the whole blade surface. This is equivalent to a flow simulation without cavity. The good agreement of CASE1 and CASE2 leads to the assumption that subsonic unsteady time-linearized solutions own a certain robustness concerning the accuracy of the steady state solution. Also, it can be deduced that an accurate modeling of cavities is vital for an accurate steady

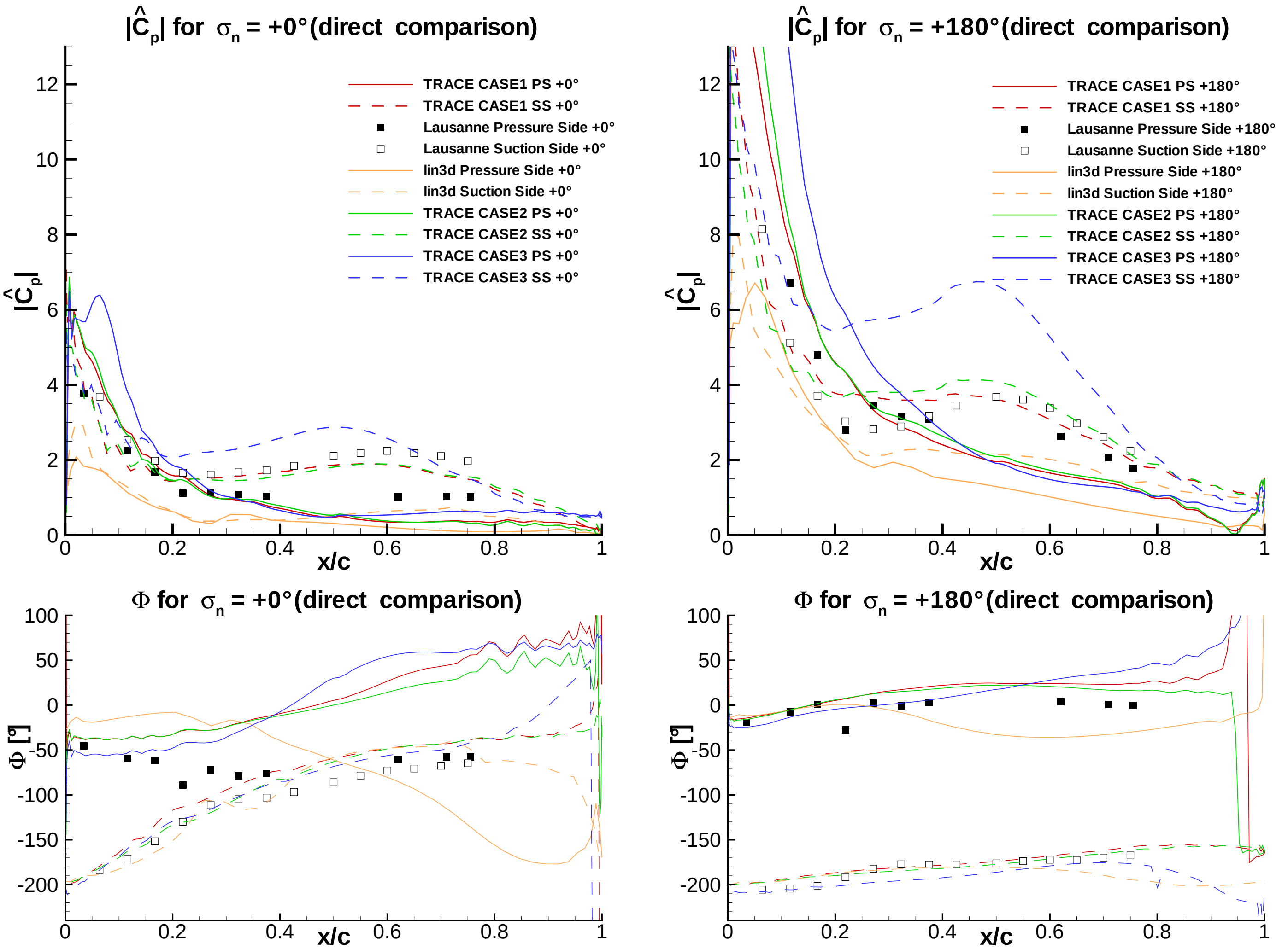

FIGURE 13. COMPARISON OF THE UNSTEADY PRESSURE OF THE THREE TEST CASES WITH THE EXPERIMENTAL DATA (SUBSONIC CASE)

state solution and therefore for meaningful time-linearized results. Even though the direct comparison in Fig. 13 reveals large discrepancies between CASE3 and experimental results, the critical IBPA range is predicted correctly. A reason for this is that phase angle and pressure amplitude are predicted reasonably well in areas with large motion amplitude ($x/c < 0.3$). This results in similar aerodynamic work integrated over the blade surface.

Transonic Case (Ma = 0.85)

For the transonic case with an average inlet velocity of Ma = 0.85, all parameter variations were carried out with cavity modeling. The same four parameters were varied in order to determine their influence on the transonic steady state solution and to obtain a solution with good agreement with the experiment. The parameters varied were:

- Leak mass flow in the cavity,
- Angle of attack,
- Inlet conditions between 0% - 15% and 85% - 100% of the channel height and
- Outlet pressure.

Steady State Simulation. A comparison of the parameter variations for the transonic case with the ones for the subsonic case shows similarities and differences:

- At first glimpse, the variation of the leak mass flow seems to have a completely opposite effect for subsonic and transonic flows (Fig. 7 & 14). This is due to the fact that the leak was

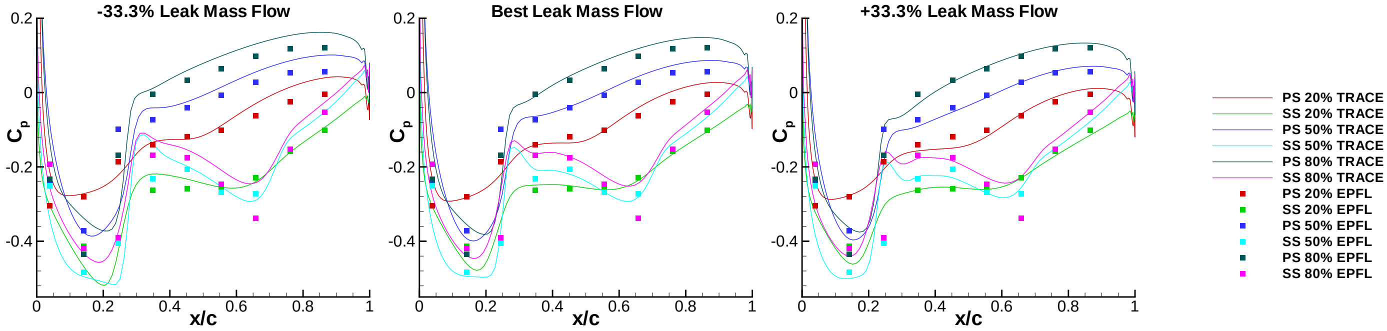

FIGURE 14. CONSEQUENCES OF A LEAK MASS FLOW VARIATION IN THE CAVITY (TRANSONIC CASE)

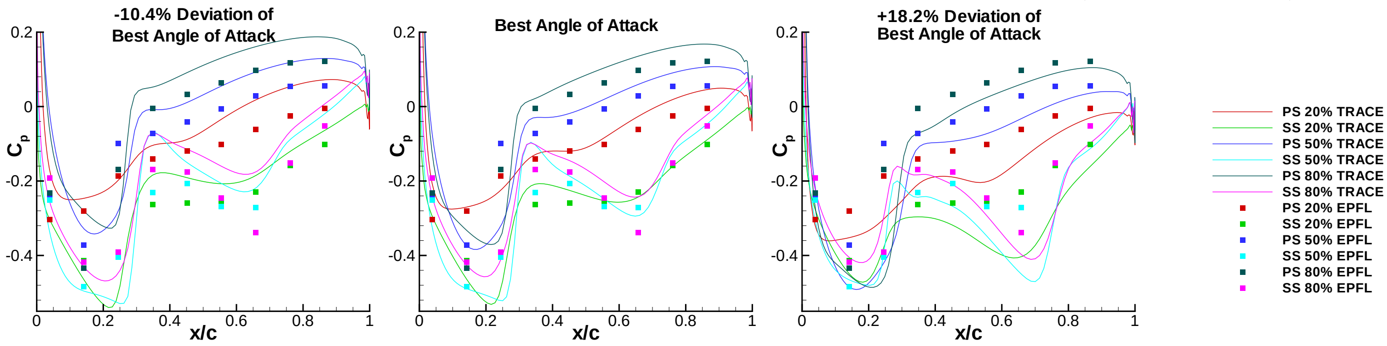

FIGURE 15. CONSEQUENCES OF AN ANGLE OF ATTACK VARIATION (TRANSONIC CASE)

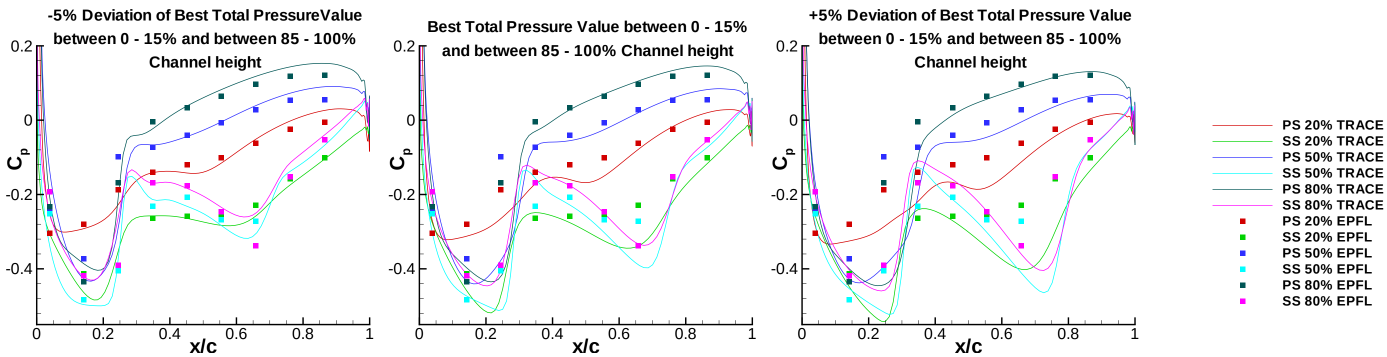

FIGURE 16. CONSEQUENCES OF A VARIATION OF THE TOTAL PRESSURE AT PARTS OF THE INLET (TRANSONIC CASE)

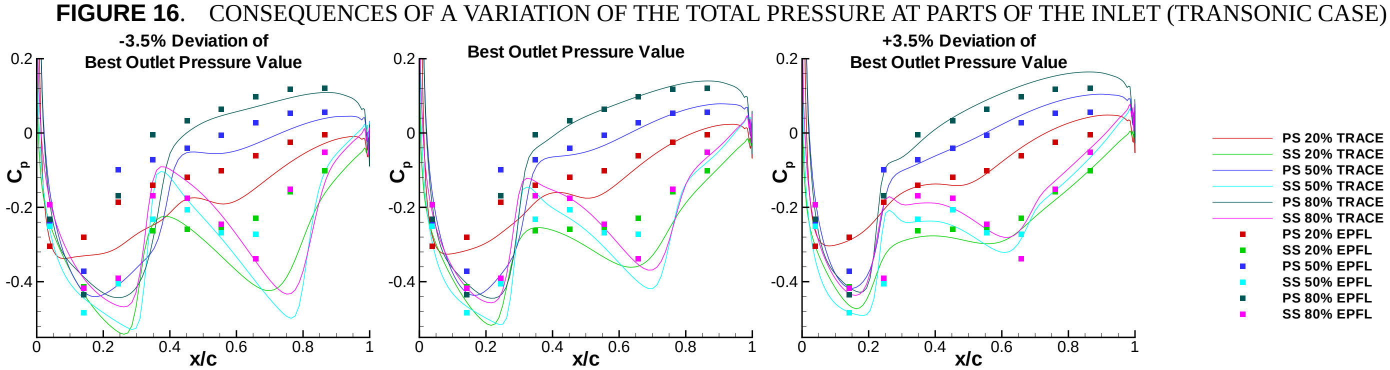

FIGURE 17. CONSEQUENCES OF AN EXIT PRESSURE VARIATION (TRANSONIC CASE)

an outlet for the subsonic case and an inlet for the transonic case. Taking this into account, the effect of the leak mass flow is the same as for the subsonic case.

- The variation of the angle of attack (Fig. 15) also results in a variation of the difference between the pressures on the pressure side and on the suction side of the blade (similar to Fig. 8). An additional effect is the variation of the shock intensity especially on the suction side of the blade (lower angle of attack, stronger shock on the suction side).
- The variation of the total inlet pressure between 0% - 15% and 85% - 100% shows the same effect as for the subsonic case (Fig. 16 & 9). This was to be expected since the inlet total pressure is a very important part of the simulation and determines the mass flow. An increased mass flow (higher total pressure at the inlet) at stable outlet pressure results in higher velocities and therefore a more prominent dip of the pressure at the front part of the blade before the shock.
- The variation of the exit static pressure (Fig. 17) is now not a pure scaling factor for the pressure on the blade surface any longer (compare to Fig. 10). Since the flow regime is transonic, an increase in velocity also results in a more intensive shock, therefore the static pressure at the outlet also influences the magnitude of the pressure leap at the shock boundary.

A similarly accurate steady state solution as for the subsonic flow case was found for the transonic flow case by combining all those four effects (Fig 19, CASE1). This solution was then used as basis for unsteady time-linearized simulations.

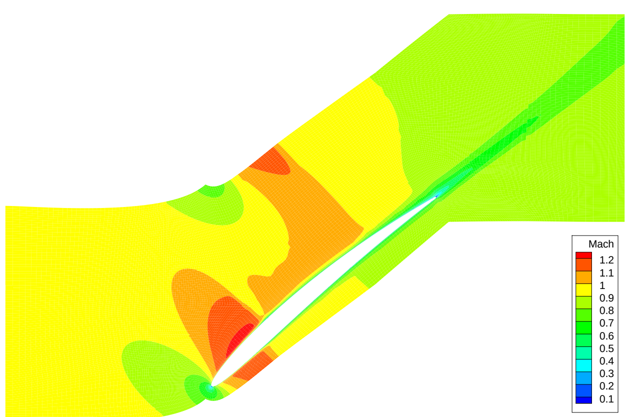

FIGURE 18. MACH NUMBER DISTRIBUTION AT 50% CHANNEL HEIGHT (TRANSONIC CASE)

Also for this flow case, the authors assumed that the constant eddy viscosity assumption holds true for the flow around the profile. In Fig. 18, the supersonic regions as well as the shocks arising are clearly visible. Even though the boundary layer thickens towards the trailing edge, an unseparated flow prevails.

Unsteady Time-Linearized Simulations. The time-linearized transonic simulations were performed similarly to the subsonic ones. CASE1 is the simulation based on the best steady state solution obtained with the parameter variations. CASE2 is a time-linearized simulation based on a steady state solution with less accurate inlet (+5% deviation of total pressure between 0% - 15% and between 85% - 100% channel height compared to CASE1; no angle of attack variation) and outlet conditions (-2.8% deviation of static pressure value from CASE1) as well as without leak mass flow, and CASE3 is equal to CASE2 but without cavity modeling.

Figure 22 shows the unsteady pressure distribution at 50% channel height in amplitude and phase angle for those three cases, the Lin3D comparison case and the experimental values for the IBPAs 0° and 180°. At first glance, there seem to be large discrepancies between all simulated results and the experiment for the unsteady pressure distribution. The unresolved peaks located at the shock locations can be explained by two things. On the one hand, the transonic steady state solution is very sensitive for inlet and outlet conditions. Therefore the position of the shock of the transonic steady state solution might have been a little off. On the other hand, the pressure sensors were spaced widely, therefore the peaks of the unsteady pressure distribution were not resolved accurately enough (Shock beside the pressure sensor, therefore no representation of the high unsteady pressure values caused by the shock oscillation). Bearing this in mind and comparing the phase angle between blade motion and pressure fluctuation Φ, a similar conclusion can be drawn as for the subsonic case: for IBPA 180°, CASE1 delivers very accurate unsteady results, with CASE2 and CASE3 deviating more and more from the experimental values. The Lin3D comparison based on the best steady state solution delivers once again results in the accuracy range of CASE2.

Similarly to the subsonic case, Φ is not calculated correctly for the pressure side at IBPA 0°. There are several explanations for this observation: Firstly, due to instrumentation, the measurements have been performed on 4 different blades and were corrected by the IBPA of the experiment. If the IBPA in the experiment was slightly different from blade to blade this would introduce an error. Secondly, the pressure amplitudes for $x/c > 0.5$ are rather small, especially for the transonic case. On the one hand, this makes it difficult to determine the corresponding phase angles correctly. On the other hand, small deviations in simulation and/or experiment might change the sign of the complex pressure value, which would be equivalent to a phase difference of 180°.

A comparison of the logarithmic decrement of aerodynamic damping Λ_{AERO} for those five cases (Fig. 20) shows that unsteady

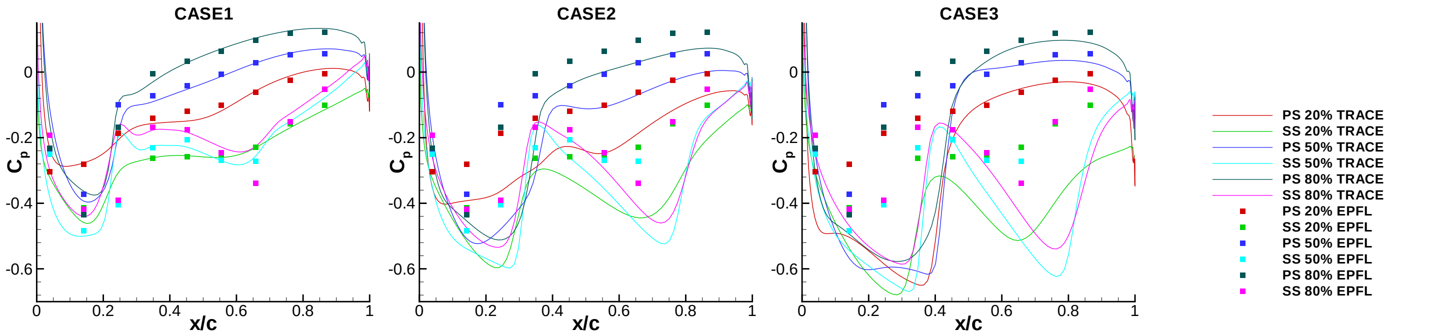

FIGURE 19. BEST CASE (CASE1), LESS ACCURATE CASE (CASE2) AND LESS ACCURATE CASE WITHOUT CAVITY MODELING (CASE3) (TRANSONIC CASE)

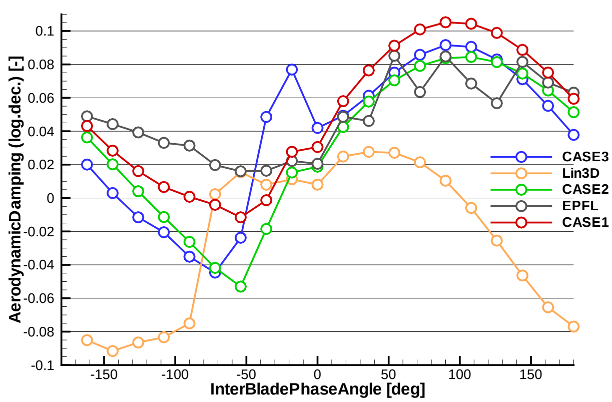

FIGURE 20. COMPARISON OF THE LOG.-DEC. OF AERODYNAMIC DAMPING OF THE FOUR TEST CASES (TRANSONIC CASE)

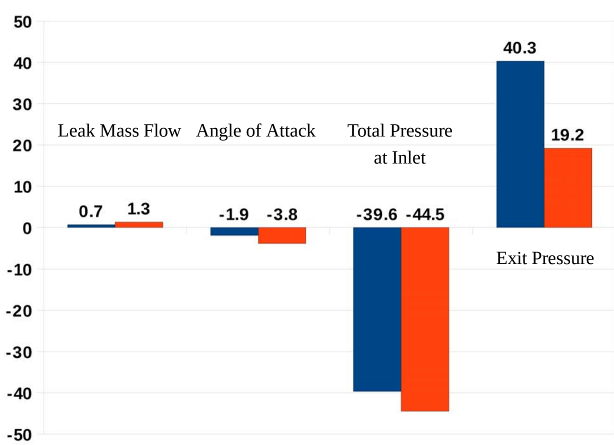

FIGURE 21. SENSITIVITY OF AERODYNAMIC DAMPING FOR THE TRANSONIC CASE

time-linearized simulations of transonic flow cases are very sensitive concerning the steady state solution on which they are based. For example, there seems to be a large influence of the position and the strength of the shock. In CASE1, the shock is at the front of the blade and of intermediate intensity. For CASE2, the shock has moved further downstream and has become stronger. In CASE3, a complicated transonic shock system has emerged. This is reproduced for the unsteady pressures in Fig. 22, since shock motion is responsible for the unsteady pressure peaks.

Integrated over the whole blade surface, this results in great differences for the aerodynamic damping (Fig. 20). Even though CASE2 still predicts the critical IBPA range correctly, its magnitude there is very different to the solution of CASE1. The results of CASE3 also predict the critical IBPA range correctly, but show large discrepancies for one discrete IBPA. Additionally, the IBPA with the smallest aerodynamic damping has moved. The Lin3D code delivers very different predictions in the transonic range.

Sensitivity of Aerodynamic Damping For the transonic case, further time-linearized computations have been performed for the critical IBPA range (7 nodal parameters) by varying the four parameters leak mass flow, angle of attack, total inlet pressure and static outlet pressure. Taking into account the IBPA with the minimum aerodynamic damping and its direct neighbors, sensitivities for this aeroelastic stability parameter have been deduced.

Figure 21 shows the sensitivity of the minimum aerodynamic damping with respect to the mentioned parameters: values of the blue and red bars are computed from the parameter diminuation and augmentation respectively (left and right columns in the steady state solutions of Figs. 14 - 17 respectively).

As can be seen, the sensitivity with regard to leak mass flow and angle of attack is very small. That is to say, big changes are required for a significant shift of the global aerodynamic damping. However, the total pressure ratio between outlet and inlet

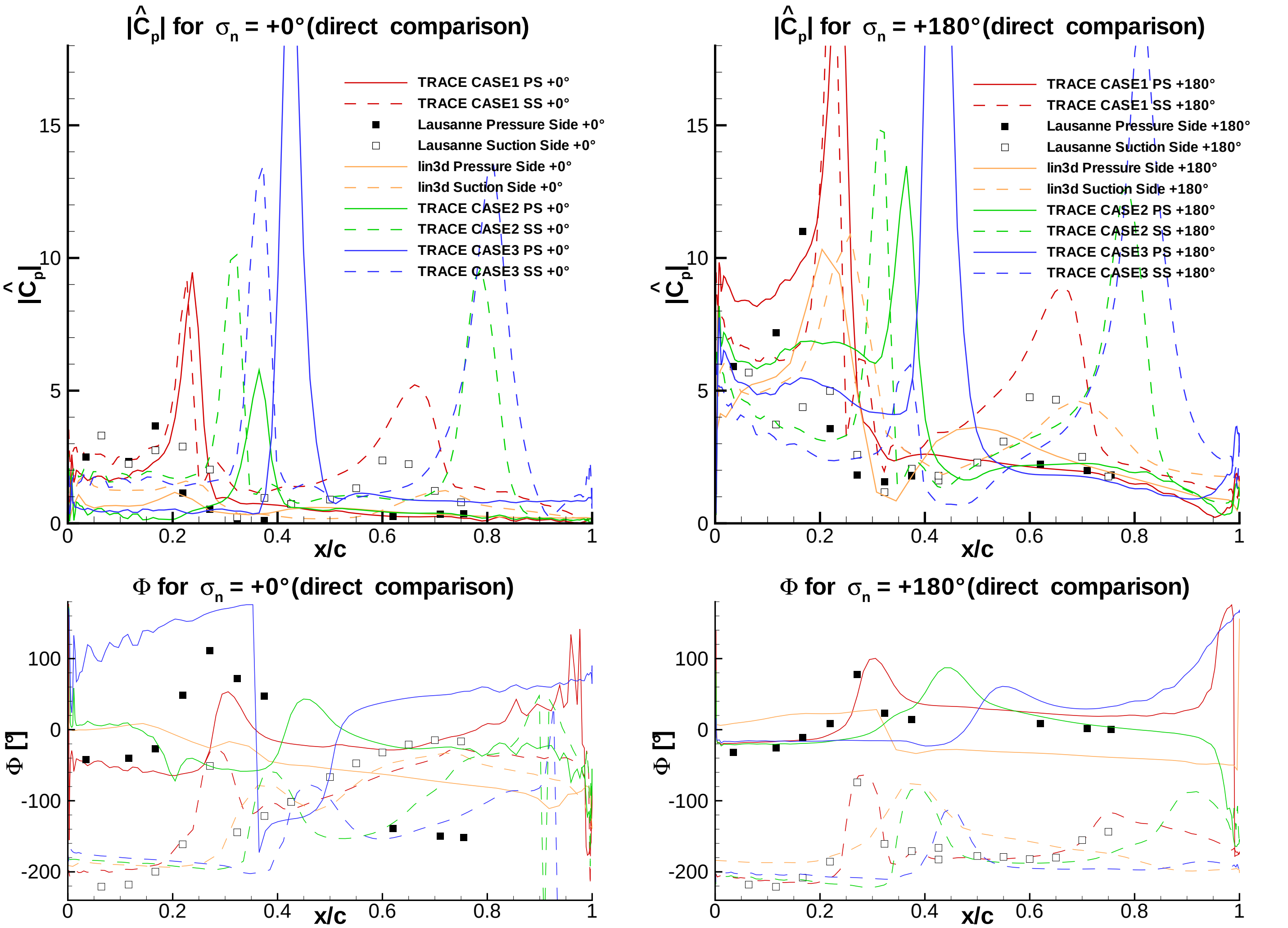

FIGURE 22. COMPARISON OF THE UNSTEADY PRESSURE OF THE THREE TEST CASES WITH THE EXPERIMENTAL DATA (TRANSONIC CASE)

plays the decisive role: It can be augmented by lower total pressure values at the inlet or higher static pressure values at the outlet. Changing these values by 1% in the respective direction leads to an augmentation of the aerodynamic damping by about 40% and vice versa. This means that changing one of these values by 2.5% in the other direction can cause a complete loss of the aerodynamic stability margin.

CONCLUSION

The influence of the steady flow solution on the aeroelastic stability behaviour of an annular compressor cascade has been studied in order to find margins for acceptable deviations in terms of steady pressure distribution that do not immediately deteriorate the accuracy of the unsteady simulation. In this context two different flow regimes - a subsonic and a transonic case - were subject to the analysis.

The pressure distributions on the blade surface of a NACA3506 profile were compared to experimental data that has been gained by the Institute of Aeroelasticity of the German Aerospace Center (DLR) during several wind tunnel tests at the annular cascade facility RGP-400 of the Ecole Polytechnique Fédérale de Lausanne.

The influence of the parameters inlet total pressure, outlet static pressure, leak mass flow in a cavity and angle of attack were examined. It became clear that even small deviations from the real values of those parameters show a large effect on the steady state solution.

The importance of cavity modeling was highlighted and it could be concluded that it is imperative to model large cavities to obtain accurate steady state solutions.

On the basis of three differently accurate steady state solutions for a subsonic and a transonic case respectively, unsteady time-linearized simulations were run and their accordance with the experimental results was investigated. It was concluded that subsonic flow cases own a certain robustness concerning the accuracy of the steady state solution which the unsteady time-linearized simulation is based on. Contrary to this, it is of utmost importance to use steady state solutions that are as accurate as possible to run transonic unsteady time-linearized simulations because their results are dominated by position and motion of the shock. If the shock position is not captured correctly in the steady state solution, the big work entries due to its motion may lead to a wrong evaluation of flutter stability.
This is underlined by the sensitivities of the aerodynamic damping determined for the transonic case. The total pressure ratio between outlet and inlet is the driving force and has to be adjusted very thoroughly in the steady state solution in order to produce reliable time-linearized results.

ACKNOWLEDGMENT

The authors would like to thank MTU Aero Engines GmbH for the permission to publish the contents of this work as well as their colleagues from the DLR Institute of Propulsion Technology for providing the TRACE code.

Special thanks go to Dr. Joachim Belz for his support concerning the post-processing of the experimental data from the measurements at EPFL.

REFERENCES

[1] Hall, K., 1987. "A Linearized Euler Analysis of Unsteady Flow in Turbomachinery". PhD thesis, MIT Cambridge, USA.

[2] Holmes, D., and Lorence, C., 1998. "Three-Dimensional Linearized Navier-Stokes Calculations for Flutter and Forced Response". In *Unsteady Aerodynamics and Aeroelasticity of Turbomachines*, T. Fransson, ed. Kluwer Academic Publishers, pp. 211–224.

[3] Clark, W., and Hall, K., 2000. "A Time-Linearized Navier-Stokes Analysis of Stall Flutter". *Journal of Turbomachinery,* ***122***(3), pp. 467–476.

[4] Sbardella, L., and Imregun, M., 2001. "Linearized Unsteady Viscous Turbomachinery Flows Using Hybrid Grids". *Journal of Turbomachinery,* ***123***(3), July, pp. 568–582.

[5] Campobasso, M., and Giles, M., 2002. "Stabilization of a Linearized Navier-Stokes Solver for Turbomachinery Aeroelasticity". In *Computational Fluid Dynamics 2002*.

[6] Platzer, M., and Carta, F., eds., 1987/88. *Aeroelasticity in Axial-Flow Turbomachines*, Vol. Volume 1: Unsteady Turbomachinery Aerodynamics. Volume 2: Structural Dynamics and Aeroelasticity of *AGARDograph No. 298*. AGARD.

[7] Lane, F., 1956. "System Mode Shapes in the Flutter of Compressor Blade Rows". *Journal of Aeronautical Sciences,* ***23***, January, pp. 54–66.

[8] Hagenah, B., 2004. "Development and Application of a time-linearized 2D Euler Solver for Flutter Investigations in Turbomachines". PhD thesis, RWTH Aachen, Germany.

[9] Petrie-Repar, P., 2003. "Development of an Efficient and Robust Linearised Navier-Stokes Flow Solver". In 10th International Symposium on Unsteady Aerodynamics, Aeroacustics and Aeroelasticity of Turbomachines (ISUAAAT).

[10] Kersken, H.-P., Frey, C., Voigt, C., and Ashcroft, G., 2010. "Time-Linearized and Time-Accurate 3D RANS Methods for Aeroelastic Analysis in Turbomachinery". In Proceedings of ASME Turbo Expo 2010 in Glasgow, UK. Paper No. GT2010-22940.

[11] Kahl, G., 2002. "Aeroelastic Effects of Mistuning and Coupling in Turbomachinery Bladings". PhD thesis, EPF Lausanne, Switzerland.

[12] Bölcs, A., 1983. "A Test Facility for the Investigation of Steady and Unsteady Transonic Flows in Annular Cascades". In *ASME Paper 83-GT-34*.

[13] Belz, J., and Hennings, H., 2000. "Aerodynamic Stability Investigations of an Annular Compressor Cascade Based on Unsteady Pressure Measurements". In Proceedings of the 9th International Symposium on Unsteady Aerodynamics, Aeroacustics and Aeroelasticity of Turbomachines (ISUAAAT), pp. 280 – 295.

[14] Belz, J., Hennings, H., and Kahl, G., 2010. "Experimental Investigation of the Forcing Function and Forced Pitching Blade Oscillations of an Annular Compressor Cascade in Transonic Flow". In Proceedings of ASME Turbo Expo 2010: Power for Land, Sea and Air (GT 2010).

[15] Franke, M., Kügeler, E., and Nürnberger, D., 2005. Das DLR-Verfahren TRACE: Moderne Simulationstechniken für Turbomaschinenströmungen. Tech. rep., Institute of Propulsion Technology, DLR.

[16] Kemme, R., 2004. "Numerische Untersuchungen zum aeroelastischen Verhalten eines hochbelasteten Verdichterrotors". PhD thesis, Universität Hannover.

[17] Kahl, G., and Hennings, H., 2000. "Computational Investigation of an Oscillating Compressor Cascade Experiment". In Proceedings of the 9th International Symposium on Unsteady Aerodynamics, Aeroacustics and Aeroelasticity of Turbomachines (ISUAAAT), pp. 819 – 829.